Colloid Polym Sci (2002) 280: 973–983
DOI 10.1007/s00396-002-0715-y

ORIGINAL CONTRIBUTION

Marcia Bragato
Günter Subklew
Milan J. Schwuger
Omar A. El Seoud

Vegetable oils-based microemulsions: Formation, properties, and application for "ex-situ" soil decontamination

Received: 7 February 2002
Revised: 5 April 2002
Accepted: 8 April 2002
Published online: 11 June 2002

M. Bragato · O.A. El Seoud (✉)
Instituto de Química, Universidade de São Paulo, C.P. 26077, 05513–970, São Paulo, S.P., Brazil
E-mail: elseoud@iq.usp.br
Fax: +55-11-3091-3874

G. Subklew · M.J. Schwuger
Forschungszentrum Jülich GmbH, Institut für Angewandte Physikalische Chemie, 52425-Jülich, Germany

Abstract Methyl esters of coconut oil (CME) and the saturated fraction of palm oil (PME) were prepared from precursor oils by transesterification. Phase diagrams of oil (CME or PME)/water/non-ionic surfactant (Synperonic 91/4) were studied as a function of system composition and temperature. Rheology measurements and X-ray diffraction of the monophases obtained indicated that they are free of cubic liquid crystals. Quasi-elastic light scattering and interfacial tensions of these monophases indicated that they are either bi-continuous, or W/O microemulsions, μEs. Both types were used in decontamination of soil impregnated with polycyclic aromatic hydrocarbons, PAHs. CME- and PME-based μEs (at 37.5 °C, and 42.5 °C, respectively) were found to be more efficient decontaminators than hot toluene. This is attributed to desorption of the contaminants by the μE, followed by their solubilization. The surface charge density of the soil (an indicator of its bioavailability) increased by a factor of 1.6 and 1.8 after decontamination by CME- and PME-based μEs, respectively.

Introduction

Polycyclic aromatic hydrocarbons (PAHs) and polychlorinated biphenyls (PCBs) are notorious, difficult-to-remove contaminants due to their strong adsorption on soil particles. For example, the pesticide Lindane (hexachlorocyclohexane) binds strongly to clays [1] and humic substances [2]. Soil remediation techniques are generally classified into "in-situ" and "ex-situ". The former technique includes injection of extraction fluids into the soil, followed by their removal by pumping [3]. In the "ex-situ" process, contaminated soil is excavated and treated either on- or off-site, then re-deposited [4]. This scheme is particularly suitable for soil remediation of relatively small, highly contaminated areas, such as dumping sites of chemical plants.

Independent of the technique employed, soil treatment may be biological, chemical, physical, or a combination of these methods. Biological treatment depends on the ability of microorganisms to biodegrade the pollutants and tolerate their toxicity [5, 6]. Examples of chemical treatments are oxidation (including incineration), chelation, and neutralization [7]. Soil flushing with air or water are physical methods of limited decontamination efficiency. Washing the soil with dilute aqueous surfactant has been applied on a pilot scale. Low solubilities of PAHs and PCBs in these solutions, and the need to treat large volumes of contaminated micellar solutions are unattractive features of this method. Nevertheless, their ability to remove dense organic liquids from contaminated soil has been recently shown [8].

There is an intense interest in soil decontamination by microemulsions, μEs. These are transparent or translucent liquids containing at least three components, namely, surfactant (S), oil (O), and water (W). Depending on the continuous phase, they are classified into O/W μEs, bi-continuous μEs, or W/O μEs. They are isotropic and thermodynamically stable under a specified set of experimental conditions. Although changing these conditions (e.g., the temperature) may lead to

phase separation, they reform *spontaneously* once the original conditions are restored.

Soil remediation by μEs is an attractive technique due to the following features: (i) decontamination efficiency is high because the μE decreases the pollutant/soil interfacial tension to very low values [9]; desorbed contaminants then easily dissolve in the μE; (ii) the volumes handled are much smaller than those produced in decontamination by aqueous micellar solutions; (iii) separation of the μE into a surfactant-rich aqueous phase (for recycling) and an organic phase containing the contaminants (for disposal) is simply achieved by changing the temperature of the μE (vide infra).

A recently introduced "ex-situ" soil decontamination process is depicted in Scheme 1. It involves the following steps: a) extraction of the contaminated soil with the μE; b) separation of the soil from the μE; c) temperature change-induced separation of the μE into two phases: oil containing dissolved pollutants, and a surfactant-rich aqueous phase; d) disposal of the oil phase (e.g., by biodegradation or incineration) and recycling of the aqueous phase into the process; e) washing and re-deposition of decontaminated soil [10, 11, 12]. Environmental restrictions dictate that the surfactant and oil components of the μE should be biodegradable, this being the reason for using vegetable and not mineral oils.

Application of this scheme requires a better understanding of the formation and properties of vegetable oil-based μEs. More information is required on the relative importance of the variables involved: μE composition, average structure of the vegetable oil employed, and temperature. Previous results have shown that methyl or ethyl esters of vegetable oils form μEs at lower temperatures than the precursor oils, probably because of steric factors [10, 11, 12].

We report here on the formation, properties, and soil decontamination by μEs based on methyl esters of two vegetable oils (hereafter designated as "oils"), namely coconut oil (CME) and the saturated fraction of palm oil (PME). Phase diagrams were determined as a function of system composition and temperature, followed by determination of microstructures of the single-phase regions. Our results showed that CME and PME form μEs close to room temperature; these are more efficient decontaminators than their rapeseed oil (RME)-based counterparts [10, 11, 12].

Experimental

Materials

All reagents were purchased from Aldrich or Merck and were purified as reported elsewhere [13]. Food-grade coconut oil (*Cocos nucifera*) and palm oil (*Elaeis guineensis*) were purchased from Almadi Alimentos (São Paulo, Brazil). Chromatographic standards for the analysis of fatty acid composition of CME and PME were from Polyscience (Niles, USA). The solvatochromic probe 2,6-dichloro-4-(2,4,6-triphenyl-1-pyridinio)-phenolate was synthesized according to a method given elsewhere [14].

The non-ionic surfactants tested were the following commercial linear alkylpolyethoxylates: Synperonic 91/4, $CH_3(CH_2)_{8-10}(OCH_2CH_2)_4OH$, Synperonic 91/5, $CH_3(CH_2)_{8-10}(OCH_2CH_2)_5OH$ (ICI, Middlesborough, UK) and Marlipal 24/50, $CH_3(CH_2)_{11-13}(OCH_2CH_2)_5OH$ (Hüls, Marl, Germany). Each of these surfactants is a *blend*; HPLC analyses have indicated that the alkyl moiety of the Synperonic 91 series is 35% $CH_3(CH_2)_8$- and 65% $CH_3(CH_2)_{10}$-,

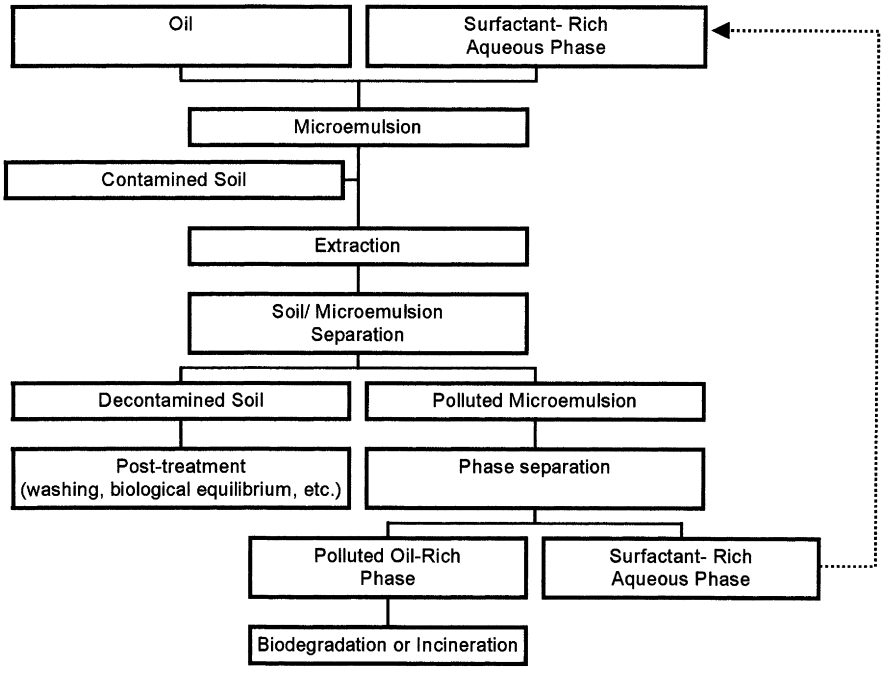

Scheme 1. Flow diagram of soil decontamination by microemulsions

whereas that of Marlipal 24/50 is 75% $CH_3(CH_2)_{11}$- and 25% $CH_3(CH_2)_{13}$- [15].

PAH-contaminated soil (hereafter designated "soil") was obtained from Forschungszentrum Jülich (Jülich, Germany). Its organic matter and PAHs contents were found to be 13.5% and 3600 ppm (Soxhlet extraction with toluene, 6 hours), respectively. Tonsil Optimum 210FF Ca-bentonite clay (Süd Chemie, Munich, Germany) was used as received.

Preparation and characterization of CME and PME

These methyl esters were prepared by transesterification (sodium methoxide/methanol) of the appropriate oil [16, 17, 18]. Palm oil methyl esters were separated into a saturated-rich fraction, PME, and an unsaturated-rich one, as follows: the mixture obtained by transesterification was centrifuged at 4.0 ± 0.1 °C, at 4280 *g* for 30 minutes. The solid fraction obtained (PME) was separated and then bleached by heating at 40 °C under nitrogen atmosphere for 2 hours with 0.5% of the Tonsil Optimum clay (w/v). The esters obtained were kept under nitrogen at approximately 5 °C in tightly-stoppered polyethylene bottles.

The esters were characterized by the following American Oil Chemists Society official methods: Acid value, OM Cd 3a-63; Iodine value (Wijs), OM RP Cd 1b-87; Peroxide value, OM Cd 8–53; Saponification value, OM Cd 3–25; Fatty acid composition, OM Ce 1–62 (GC analysis) [19]. We used a model GC 17A-2 gas chromatograph (Shimadzu, Kyoto, Japan), equipped with FID detector and Supelcowax 10 capillary column (Supelco, Bellefonte, USA). The analysis conditions were: injector temperature 230 °C; FID temperature 260 °C; column heating rate 10 °C min^{-1} until 160 °C then 5 °C min^{-1} until 240 °C; carrier gas N_2; split ratio 1:50.

Phase diagrams

Pseudo-ternary phase diagrams were constructed as follows: Surfactant, water, and oil were accurately weighed in Pyrex tubes with Teflon-lined caps. The tubes were tightly closed, the contents were thoroughly mixed (vortex tube mixer, 1 min), and placed in a thermostated bath at the desired temperature until phase equilibrium was reached (several hours to days). The number and appearance of phases was noted (using crossed polarizers to detect liquid crystalline phases). The tubes were then submitted to another cycle of mixing/thermostating at a new, lower temperature. We used 5 or 2.5 °C intervals when there was a change in the number of phases [20, 21]. After definition of the phase diagram, compositions that showed two phases were repeated to determine the nature of the main component of each phase, that is, W or O. Two samples were prepared for each composition, one contained a water-soluble dye (10^{-5} M methylene blue) the other contained an oil-soluble dye (10^{-5} M Sudan IV). The main component of each phase was deduced from volumes of the aqueous phase (blue) and the oil phase (red).

Characterization of the monophases

The monophases obtained were characterized by rheology, X-ray diffraction, quasi-elastic light scattering, QELS, interfacial tension, IFT, and contact angle (θ).

Rheological measurements

The viscosities and rheological behavior of the pure components (O and S) and the monophases were studied as a function of temperature ($35.0–45.0 \pm 0.1$ °C), time (0–6 min), and shear rate (75–450 s^{-1}) with model LV-III, cone/plate rheometer (Brookfield, Stoughton, USA). The uncertainty in the viscosities determined was $\leq$ 1%.

X-ray diffraction

A home-built X-ray diffractometer operating in the Laue transmission geometry was used. The apparatus includes model 4057A2 X-ray generator (40 kV, 30 mA, Cu-Kα radiation, Rigaku, Tokyo, Japan), graphite monochromator, and a film for registering the X-ray diffraction. The μE sample was placed into a 2.0 mm capillary, centrifuged, and then introduced into the cell compartment whose temperature was kept constant within ± 0.2 °C.

Quasi-elastic light scattering

The apparent diffusion coefficient (D) of the μE nanodroplets was determined by model 4700 MW light scattering system (Malvern, Worcestershire, UK), equipped with a 25 mW He/Ne laser source (Spectra Physics, Mountain View, USA) and 256 channel autocorrelator. The sample was directly filtered into the measurement cell (0.45 μm filter) and left for 15 minutes for thermal equilibration. Each autocorrelation function was an average of ten measurements, and the results were analyzed by the cumulants method [22, 23]. The autocorrelation function of the scattered intensity is related to the apparent diffusion coefficient by:

$$G(q,\tau) = A\left[1 + B\exp\left(-2q^2 D\tau c\right)\right] \quad (1)$$

Where the scattering vector (q) is given by $q = (4\pi n/\lambda_o)\sin(\theta/2)$, A is the square of the intensity of scattered light, and B is an instrument constant. In the definition of q, n is the refractive index of the sample, λ_o is the wavelength of the laser light (632.8 nm), θ is the scattering angle (90°), and τ is the sample correlation time. Normalized diffusion coefficients (D_n) were calculated from the equation:

$$D_n = D\eta/T \quad (2)$$

Where T is the absolute temperature and η is solvent viscosity [22, 23]. The sample refractive index was determined with an Optilab 903 interferometric refractometer (Wyatt, Santa Barbara, USA) equipped with a He/Ne laser light source.

Interfacial tension measurements

Interfacial tensions (IFT) were determined with a Site-4 spinning-drop tensiometer (Krüss, Hamburg, Germany), and were measured as follows: after complete phase separation at the desired temperature, the appropriate two-phase system was inserted in the capillary tube of the equipment, allowed to thermally re-equilibrate, then its IFT was measured [24]. For comparison, we have repeated measurements on heptane/aqueous NaCl/ sodium dodecyl sulfate μE systems, and obtained IFT results similar to those reported elsewhere [25]. Densities were determined with a Paar DMA 40 digital densimeter (Anton Paar, Graz, Austria).

Contact angle

After complete phase separation at the desired temperature, the contact angle of the μE drop (8 μL) was measured as recommended elsewhere [26] with a home-built apparatus equipped with a QV-10 LCD digital camera (Casio, Tokyo, Japan). Due to the low angles obtained, only the advanced contact angle was measured ($\pm 2°$) from a photograph of the μE drop over the substrate (a glass slide). The latter was cleaned by immersion for 20 minutes in a hot mixture of 30% hydrogen peroxide, 28% NH_4OH, and water

(1:1:4 v/v), followed by washing with water, and drying by nitrogen [27].

Physical characterization of contaminated soil

The mineral composition of the soil was analyzed with Phillips model X'pert MPD X-ray diffractometer (Cu-Kα radiation; 40 kV, 40 mA; Ni monochromator; diffraction angle 1–90°, at 0.02° (2θ) steps and 1 s step^{-1}). The soil granulometry was analyzed with a Malvern Sedigraph Mastersizer/E, using 2 mW He/Ne laser source. An aqueous suspension of the soil (0.5 g L^{-1}) was magnetically stirred for 8 h without a defloculant, then immediately analyzed. The surface area of the soil was determined by the BET method, according to ASTM–B4567/94 designation, employing BET porosimeter model ASAP 2010 (Micromeritics Equipment, Norcross, USA) [28]. The specific surface area measured was found to be 8.8 ± 0.2 m^2 g^{-1}.

Soil decontamination by microemulsions: Capacity of extraction of PAHs

Pre-prepared μE was added to the contaminated soil, the contents were thoroughly mixed (vortex tube mixer, 2 min) and left at a constant temperature for the required contact time. The contents were centrifuged at 4280 *g* for 15 minutes. PAHs concentration was then determined in the supernatant. Blank samples, that is, without the soil, were run in parallel.

The contaminant concentration in the supernatant was determined spectrophotometrically, with a Beckman DU-70 UV-vis spectrophotometer, by measuring its absorbance at $\lambda = 333$ nm. Beer's Law plots were constructed with solutions of the solid material that was obtained by exhaustively extracting contaminated soil with hot toluene (6 hours, Soxhlet). All samples were diluted with anhydrous ethanol.

Properties of decontaminated soil

After soil/supernatant separation, the former was stirred with water for 2 hours (water/soil ratio = 10, w/w) then centrifuged at 4280 *g* for 30 minutes. After two more washing cycles, the soil sample was dried under reduced pressure at room temperature until constant weight. Its surface area was determined by the BET method, vide supra, whereas its cation exchange capacity (CEC) was determined by the methylene blue adsorption method [29, 30].

Results and discussion

Choice of system components

From the application point of view, the use of a homogeneous non-ionic surfactant (one with a *single* hydrophobic chain and a single oxyethylene moiety, e.g., $C_{12}H_{25}EO_4$) and *single* oil, e.g., methyl laurate, is prohibitively expensive. Therefore, we used commercial non-ionic surfactants and methyl esters of two vegetable oils. The general structure of the former is C_iEO_j, where the subscripts *i* and *j* refer to the *average* number of carbon atoms in the surfactant hydrophobic chain and the *average* number of oxyethylene units in its hydrophilic moiety, respectively. The average structures are $C_{9/11}EO_4$, $C_{9/11}EO_5$, and $C_{12/14}EO_5$, and their HLB values are 10.5, 11.6, and 10.6, for Synperonic 91/4, Synperonic 91/5, and Marlipal 24/50, respectively. Non-ionic surfactants have been employed because: (i) μEs can be obtained with only three components, namely W, O, and S; (ii) their HLB can be adjusted by the appropriate combination of *i* and *j*; (iii) the phase diagram is governed by the temperature, and the change of spontaneous curvature of the interfacial surfactant film [31].

Phase diagrams (not shown) of CME/W/$C_{12/14}EO_5$ and PME/W/$C_{12/14}EO_5$, indicated extensive formation of lyotropic liquid crystalline phases (Lα) along with emulsions whose separation into individual phases required long times, even at high temperatures. The slow phase separation is a consequence of the longer surfactant length (e.g., relative to $C_{9/11}EO_5$, which showed phase separation) that increases the bending elastic modulus of the surfactant film. This allows the lamellar phase boundary to occur at a lower surfactant concentration, and destabilizes the μE phase [32]. Therefore, $C_{12/14}EO_5$ was not considered any further. The reason for employing $C_{9/11}EO_4$ instead of $C_{9/11}EO_5$ will become apparent later.

It is known that the physicochemical properties that are relevant to soil decontamination, for example, solution composition and temperature of phase separation, are dependent on the structure of the oil. Therefore, we used two oils, available locally and worldwide, that essentially differ in their average number of carbon atoms: 13.7 and 16.8 for CME and PME, respectively (Table 1). The physical separation of palm oil into two fractions (by cooling and centrifugation, see Experimental) has resulted in an oil, PME with a lower unsaturation than the original palm oil. Where relevant, we compare our results with those previously obtained with RME whose average number of carbon atoms is 18.6 [10, 11, 12, 33]. Finally, we used a typically difficult-to-remediate montmorillonite soil: it is highly contaminated (3600 ppm PAHs), its organic matter content is relatively high (13.5%), and its average granulometry is very small (90% < 50 μm, 50% < 10 μm).

Phase diagrams

We start our discussion by examining the phase behavior that is typically obtained with an oil (usually a *pure* hydrocarbon) and a homogeneous non-ionic surfactant, for example, $C_{12}EO_4$ (hereafter designated as single-component system). At fixed pressure, the W/O/S system is specified by setting three independent variables, namely the temperature (*T*), and two composition variables, α and γ which are conveniently defined as [34, 35, 36]:

$$\alpha = O/(O + W) \tag{3}$$

$$\gamma = S/(S + O + W) \tag{4}$$

Table 1. Characterization of CME, PME and the parent palm oil

Analysis[a]		CME	PME	Palm oil
Fatty Acid composition (%)[b]	C8:0	7.7		
	C10:0	5.2		
	C12:0	47.0		
	C14:0	19.6	0.5	0.8
	C16:0	9.9	56.6	43.8
	C18:0	1.0	5.0	5.2
	$C18:1^{\Delta 9}$	7.1	30.7	39.7
	$C18:2^{\Delta 9,12}$	2.5	7.2	10.5
	Av. Carbon No.[c]	13.7	16.8	17.1
Saponification number		240	215	202
Acidity value		0.20	0.50	0.96
Iodine value (mg KOH g^{-1} sample)		11.6	16.3	53
Perox. value (meq kg^{-1} sample)		1.2	1.8	14.5
Density at 25 °C (g mL^{-1})		0.87	0.86	0.85

[a]Official and recommended AOCS methods.
[b]Normalized values.
[c]Calculated from the composition of fatty acids and their molecular weights.

Where the concentration of all components is given in weight. If α is fixed, for example, at 0.5, then the resulting pseudo-binary phase diagram (between T and γ) has the appearance of a "fish", with "body" and "tail" that meet at a composition designated as $\tilde{\gamma}$, and a temperature (the phase inversion temperature, PIT) designated as $\tilde{T}$; see part A of Fig. 1. At a fixed γ (below 0.4 in part A of Fig. 1), an increase in T causes a change in the number and nature of phases from: O/W μE in equilibrium with excess oil phase (denoted $\underline{2\phi}$, surfactant film curves toward oil); both oil- and water-rich phases in equilibrium with a bi-continuous phase (denoted 3ϕ), and W/O μE in equilibrium with an excess water phase (denoted $\overline{2\phi}$, surfactant film curves toward water). The "fish" tail corresponds to one-phase system (1ϕ). At $\tilde{T}$, the surfactant has equal solubilities in O and W, and the system is a bi-continuous phase (surfactant film with zero spontaneous curvature). A liquid crystalline phase (Lα) may also be observed at higher γ [34, 35, 36].

Figure 1B shows that the ("fish") phase diagrams of $CME/W/C_{9/11}EO_5$ and $CME/W/C_{9/11}EO_4$ have similar shapes except that the 1ϕ region is smaller and forms at higher temperature for the former surfactant. The solubility of a non-ionic surfactant in water decreases as a function of increasing T. For homogeneous surfactants (C_iEO_j), increasing j at a constant i increases its water

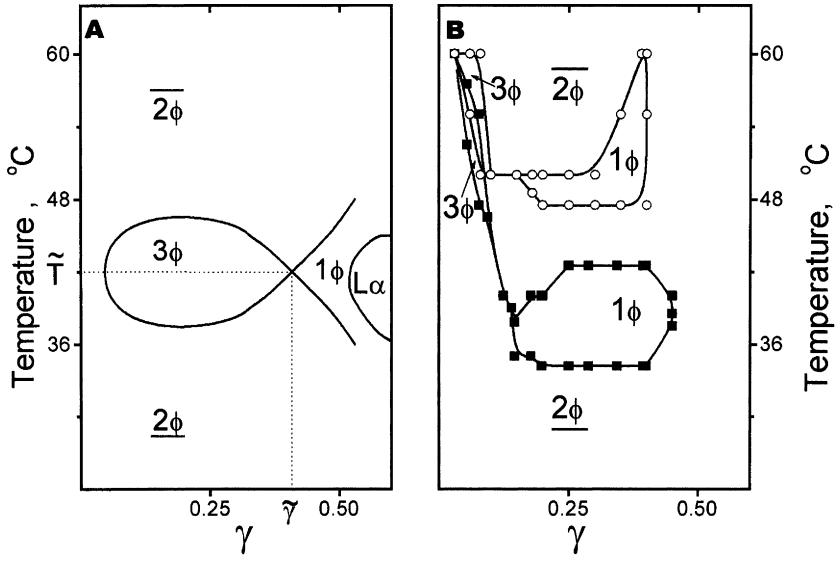

Fig. 1. A Pseudo-binary phase diagram for single-components system, redrawn from Ref. [34], and showing the "fish" with its "body" and "tail". In this and subsequent Figures, the phase symbols are 1ϕ, $\underline{2\phi}$, $\overline{2\phi}$, 3ϕ, and Lα. They refer to one phase, O/W μE in equilibrium with excess oil phase, W/O μE in equilibrium with excess water phase, oil- and water-rich phases in equilibrium with a bi-continuous phase, and lyotropic liquid crystalline phase, respectively. $\tilde{T}$ is the phase inversion temperature (PIT), the composition variables are $\alpha = O/(O+W)$ and $\gamma = S/(S+O+W)$. **B** Phase diagrams for the systems CME $/C_{9/11}EO_5/W$, (*open circles*); and $CME/C_{9/11}EO_4/W$, (■)

solubility, consequently $\tilde{T}$ increases, in agreement with part B of Fig. 1. Therefore, for soil decontamination, $C_{9/11}EO_4$ is a more interesting surfactant and it was used in the rest of our study.

Dependence of phase diagrams on the structure of oil

Relationship between γ and T

Figure 2 shows the relationship (pseudo-binary phase diagrams) between γ and T, at two fixed α, 0.5 and 0.9, for CME and PME, respectively. There are several important qualitative differences between the diagrams shown in Figs. 1A (single-components system) and 2:

1. The "fish"-type phase diagrams are severely distorted, the extension of the "fish" body is much reduced, and it is strongly skewed upward;
2. At $\alpha = 0.5$, there are two 1ϕ regions separated by Lα in equilibrium with μE;
3. At $\gamma = 0.9$, the phase diagram of CME/W/ $C_{9/11}EO_4$ bears no resemblance to that shown in Fig. 1A;
4. Stable emulsions always form at lower γ.

These differences are not surprising in view of the fact that both oil and surfactant are multi-component. In a phase diagram, the number and nature of phases depend on the distribution of surfactant between O and W. When multi-component systems are used, the conditions for formation of, for example, 3ϕ region are not easily attainable because of distribution of a series of surfactants, each with its own HLB, between water and a series of oil components, each with a different number of carbon atoms. This results in severely distorted "fish"-type phase diagrams, whose body areas are reduced compared to that depicted in Fig. 1A, as shown elsewhere (e.g., see the relevant Figs. in references [37, 38,

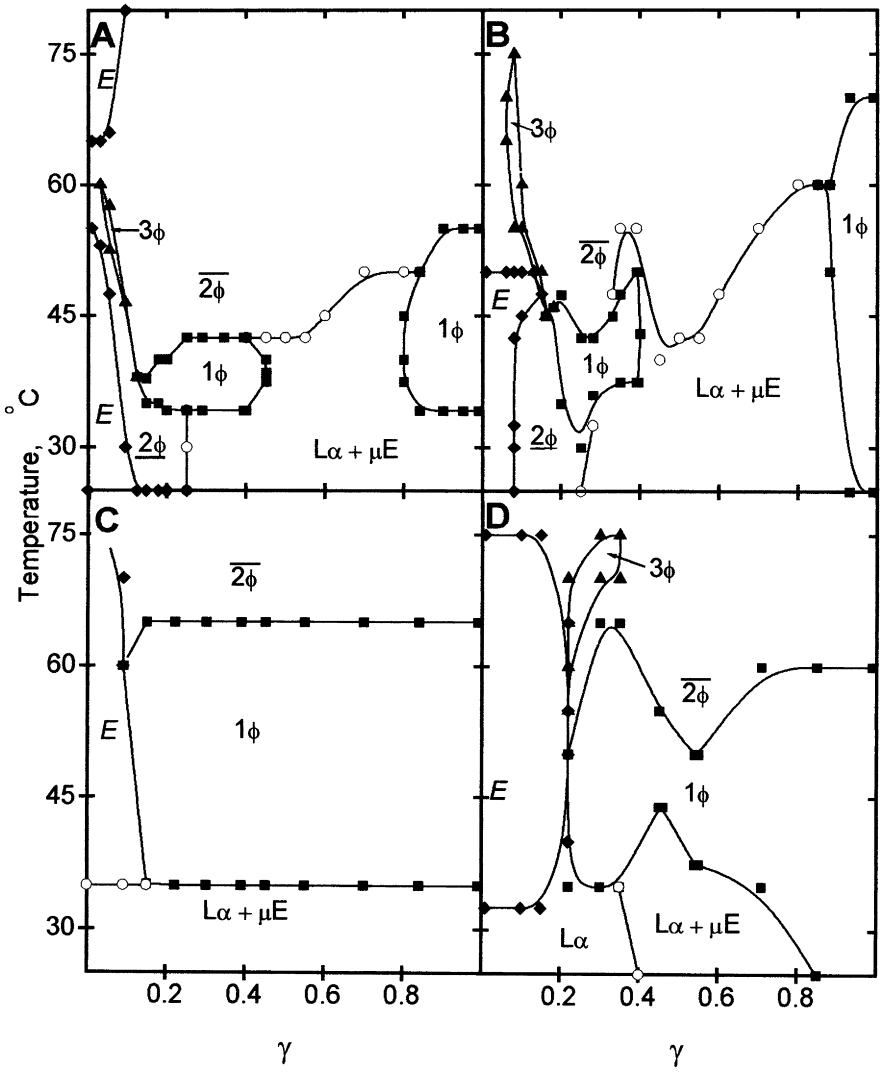

Fig. 2A–D. Pseudo-binary phase diagrams ("fish"-type diagrams) for CME/$C_{9/11}EO_4$/W (**A**: $\alpha = 0.5$; **C**: $\alpha = 0.9$) and PME/$C_{9/11}EO_4$/W (**B**: $\alpha = 0.5$; **D**: $\alpha = 0.9$). E and μE refer to a stable emulsion, and microemulsion, respectively. In this and subsequent Figures, where not specified, the symbols (e.g., *open circles*, ■, *, ▲) were drawn to guide the eye

39]). $\tilde{T}$ is usually calculated as the mean of the upper and lower temperatures of the 3ϕ region. Although calculation of $\tilde{T}$ is not feasible from Fig. 2; its value has been determined from QELS measurements, vide infra.

Relationship between α and T

Figure 3 shows the so-called "channel-cut" in the phase diagram, that is, the relationship between α and T at constant γ. Again, for comparison, part A refers to the channel cut in the phase diagram of single components system, *n*-decane/W/C_8EO_4, at $\gamma = 0.38$ [20, 21, 34, 35, 36]. The main feature of part A is the 1ϕ "channel" which goes from the lower left corner (O/W μE) to the upper right corner of the phase diagram (W/O μE). In contrast, parts B (CME) and C (PME) do not show 1ϕ system at $\alpha < 0.5$ ($\gamma = 0.3$). This is, however, not the case for RME/W/$C_{9/11}EO_4$ (phase diagram not shown) which exhibited a 1ϕ region at $\alpha < 0.5$ ($\gamma = 0.22$) [33], although the channel formed is much narrower than that shown in Fig. 3A.

These results can be explained by considering the effect of oil structure on its penetration into the surfactant film at the O/W interface, probably with its ester group pointed toward water [40, 41]. This penetration decreases as a function of increasing the oil chain length. More extensive penetration decreases the spontaneous curvature, and increases the elasticity modulus of the surfactant film. Both factors sterically constrain the curvature of the interface to favor W/O structures [34, 35, 36, 42]. That is, extensive film penetration by the shorter CME and PME oils destabilizes O/W μEs. On the other hand, the longer oil, RME, penetrates the interface to a smaller extent and affects less its curvature and elasticity, so that a narrow 1ϕ channel that extends into the O/W μE region was observed [34, 35, 36, 43].

Determination of the microstructures of the monophases

The fact that the isotropic, 1ϕ region may contain μEs (O/W, W/O, and bi-continuous) as well as cubic liquid crystals raises a question about the microstructures present in the 1ϕ regions of Fig. 2. Microstructures, however, cannot be inferred from phase diagrams alone since phase behavior patterns of several organized assemblies, for example, micelles and μEs are qualitatively similar. Therefore, we used rheology, X-ray diffraction, QELS, interfacial tension, and contact angle measurements to probe these 1ϕ regions.

With regard to the first technique, the following is relevant: (1) all 1ϕ regions exhibited a Newtonian behavior; (2) the viscosity decreases as a function of increasing α (at $\gamma = 0.3$); (3) the viscosities of the 1ϕ region of CME (18.8 mPa s at 37.5 °C) and PME (20.2 mPa s at 42.5 °C) are only 3.0 and 4.1 times greater than those calculated (from η of the individual components) for a structure-less liquid of the same composition. The results of (1) and (3) are in variance with those observed for cubic liquid crystals, which do not exhibit Newtonian behavior, and are extremely viscous [44, 45, 46]. The absence of Bragg X-ray diffraction patterns is also consistent with our conclusion that the 1ϕ regions do not contain cubic liquid crystals. This finding indicates that: QELS measurements will not be complicated, for example, by multiple scattering from cubic liquid crystals [47]; because of their low viscosities, these 1ϕ systems can be conveniently employed for soil decontamination.

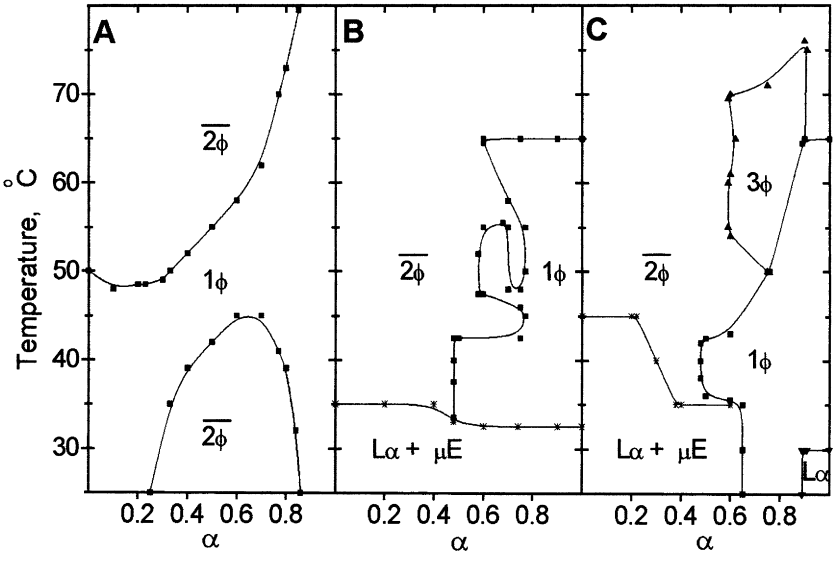

Fig. 3A–C. Pseudo-binary phase diagrams at a constant γ ("channel-cut"): **A** *n*-decane/C_8EO_4/W, $\gamma = 0.38$, redrawn from Ref. [34]; **B** CME/$C_{9/11}EO_4$/W, $\gamma = 0.30$; **C** PME/$C_{9/11}EO_4$/W, $\gamma = 0.30$

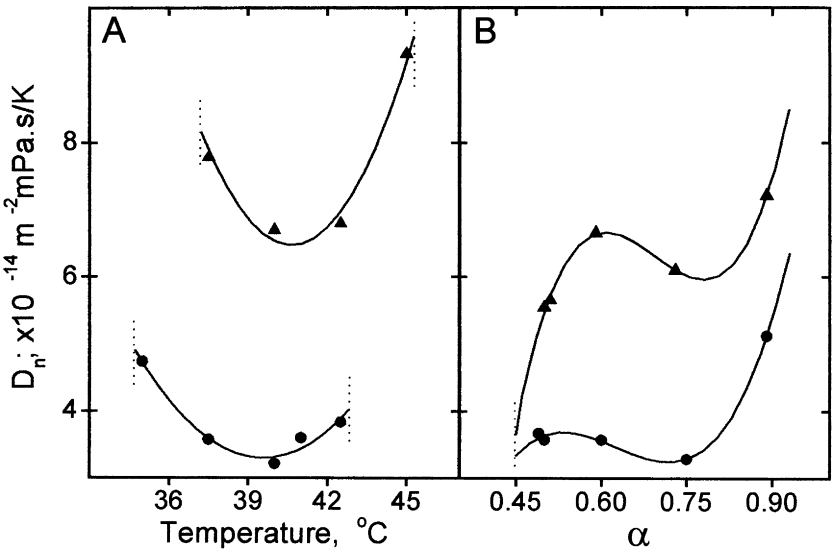

Fig. 4A,B. Dependence of the normalized apparent diffusion coefficient (D_n) on temperature (**A** at $\alpha = 0.6$ and $\gamma = 0.3$), and α (**B** at $\gamma = 0.3$), PME/ $C_{9/11}EO_4$/ W (▲); CME/$C_{9/11}$ EO_4/W, (●). The *vertical dotted lines* show the limits of isotropic phases

QELS measurements (Fig. 4) were used to show the formation of a bi-continuous phase, and to calculate the value of $\tilde{T}$ (which cannot be precisely calculated from Fig. 2). Both pieces of information were obtained from the dependence of D_n (Eq. (2) in Experimental) on conditions, namely, the temperature, part A, and α, part B. The U-shaped curve shown in part A is qualitatively similar, albeit shallower, to that observed for bi-continuous phases of a variety of single-components systems [47, 48]. The vertical lines drawn refer to the limits of the 1ϕ regions, outside of which QELS measurements were precluded by solution opalescence. The minima observed result from increase of aggregate sizes, as bi-continuous phases are approached, and are located at the PITs. Average PITs were determined after comparing the dependence of D_n on T, for all α for which 1ϕ-regions were observed, and were found to be 37.5 and 42.5 °C for RME and PME, respectively.

Figure 4B shows that D_n is rather insensitive to variation of α, around the 0.5–0.8 range. Note that D_n is related to the size fluctuation of the water- or oil-rich domains. Accordingly, our results indicate that the characteristic sizes of these domains do not vary appreciably in this α range, a result that is consistent with the presence of bi-continuous structures [43, 47, 49]. At $T \cong \tilde{T}$ the surfactant monolayers are almost planer, surrounded by relatively thick layers of water and oil. The monolayers are flexible, dynamic in nature, and undulate on a short timescale. Therefore, changes in α do not appreciably affect their structures, although the thickness of the water and oil domains vary [50]. The increase of D_n at $\alpha > 0.8$ is similar to that observed for single-components systems and is due to the formation of smaller aggregates, namely W/O μEs.

Our IFT measurements, Fig. 5 for CME, corroborate the preceding conclusion with regard to formation of bi-continuous μEs in the 1ϕ-regions. Interfacial tensions in both two-phase regions were found to be very small. Extremely small tension, approximately 10^{-6} mN m^{-1}, can be calculated by extrapolation of the curves on both sides to the 1ϕ region, in agreement with the formation of a bi-continuous μE [51, 52, 53]. Finally, the contact angles between all 1ϕ regions and glass were found to be extremely small (2–4°).

Extraction capacity of the monophase systems

In these experiments the variables are μE composition, temperature, μE/soil ratio, and contact time. Compositions close to 1ϕ boundaries were not employed because

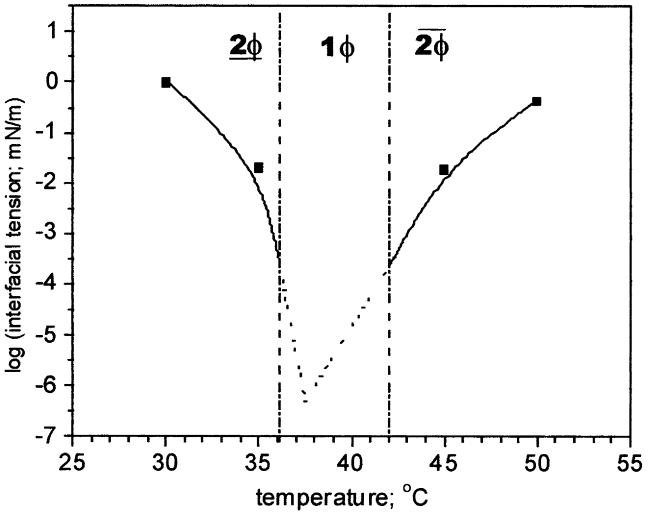

Fig. 5. Dependence of interfacial tension (IFT; between oil- and aqueous-phase) on temperature, for CME/$C_{9/11}EO_4$/W system, at $\alpha = 0.5$ and $\gamma = 0.22$. The *extrapolated* (*dotted*) *lines* intersect at "hypothetical" IFT of the 1ϕ, domain. The *vertical dashed lines* show the limits of isotropic phases

surfactant loss by adsorption may lead to phase changes, for example, from 1ϕ to 2ϕ system. From the application point of view, it is more interesting to work with μEs with low surfactant and oil contents. Figure 2 shows that the lower limit of γ is around 0.2 (α constant at 0.5); the former ratio was varied between 0.22 and 0.40. Parts B and C of Fig. 3 show that 1ϕ regions are formed at $\alpha \geq 0.5$ (γ constant at 0.3); therefore, α was varied between 0.5 and 0.9. As given elsewhere, decreasing the interfacial tension and/or contact angle between soil and the contaminant is crucial for desorption and subsequent solubilization of the latter [25, 54]. Therefore, the experiments were carried out at the PIT of each W/O/S system (where the PAH/soil interfacial tension is expected to be greatly reduced): 37.5 and 42.5 °C for CME and PME, respectively. In the following discussion we use the criterion given elsewhere [10, 11], namely, the extraction efficiency is given in %, relative to the amount extracted from the soil by hot toluene (Soxhlet, 6 hours). According to this criterion, efficiencies >100% may be obtained.

Soil decontamination is a dynamic process that depends on the type and concentration of the contaminant. Additionally, for certain soils, for example, clay-rich material, micellar solution-soil contact leads to new adsorption/desorption interlamellar equilibria for both surfactant and contaminant. These equilibria depend on the conditions employed, so that the extraction efficiency may level off, or even decrease as a function of increasing some experimental variable [55]. Therefore, we started by determining a set of optimized extraction conditions.

With regard to the optimum μE/soil ratio, we observed the following: a ratio of 4 was not sufficient to wet the whole soil; the extraction efficiency was lower at ratio of 8 than at ratio of 6. Re-adsorption of PAHs in the interlamellar spaces of the soil probably becomes significant at higher μE/soil ratios [56]. The best results were obtained at ratios of 5 or 6. Particle separation was easier at the latter ratio and it was used throughout.

We assessed the extraction efficiency of each component of the system. Soil decontamination by flushing with water, or with a 5% aqueous solution of $C_{9/11}EO_4$ were inefficient ($\leq$ 2%, contact time 1 h), whereas pure CME was much more efficient, $\leq$ 60%. The efficiency of the pure oil, which matches that of toluene at 37.5 °C is surprising and may be due to a combination of relatively low viscosity (which permits penetration into the soil pores) and high polarity, as given by the following solvent microscopic polarities, $E_T(33)$ in kcal mol^{-1}: 42.3 and 54.1, for toluene and CME, respectively [14, 57]. The oil ester group may coordinate with cations present on the soil surface; oil-soil interaction occurs at the expense of its PAH-soil counterpart, and this leads to desorption of the contaminant from the surface [58, 59].

Extraction efficiency was then examined as a function of contact time. At $\gamma = 0.3$ and $\alpha = 0.5$, the extraction efficiency reached a maximum after 3 hours contact time – after which it decreased. Therefore, the experiments were carried out at 3 hours contact time. Figure 6 shows the dependence of the extraction capacities of the μEs on α at $\gamma = 0.3$, part A, and on γ at $\alpha = 0.5$, part B.

Considering this Figure, the following is relevant:

1. The fact that an extraction capacity >100% was obtained at temperatures not far from room temperature is gratifying. At 37.5 °C, the efficiency of the μE is higher than of toluene by a factor of two. Our results also indicate that very low interfacial tensions and small angles of contact are pre-requisites for an efficient removal of PAHs;
2. The extraction efficiency decreases as a function of increasing α. That is, extraction by the bi-continuous phase is more efficient than, for example, by W/O μE;

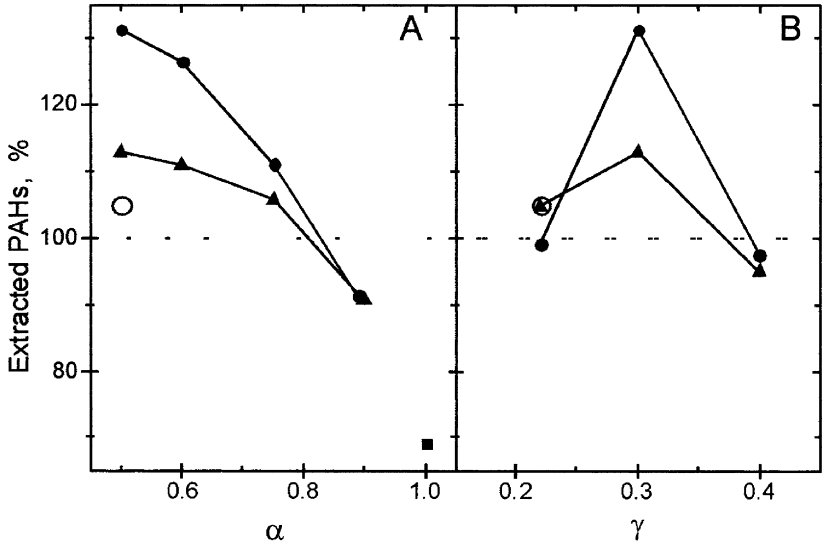

Fig. 6A,B. Extraction capacity of μEs. Contact time = 3 h, μE/soil ratio = 6. **A** $\gamma = 0.3$, **B** $\alpha = 0.5$. Data are shown for PME/$C_{9/11}EO_4$/W, 42.5 °C, (▲) CME/$C_{9/11}EO_4$/W, 37.5 °C, (●). For comparison, we included the results of extraction with toluene at 37.5 °C (■), and RME at 47 °C (*open circles*) [11]

3. The observed dependence on γ may reflect the subtle balance between the adsorption/desorption equilibria mentioned in the preceding section;
4. Extraction by μEs based on the shorter oils CME and PME is more efficient than that based on RME whose extraction figure is around 105% ($\alpha = 0.5$; $\gamma = 0.22$; $T = 43$ °C; μE/soil = 6), probably due to higher viscosity of the latter.

Finally, we have determined CEC of the decontaminated soil. This capacity bears on the bioavailability of the soil because of the required exchange of ions with plants. Surface charge density is determined (e.g., in meq m^{-2}) by dividing CEC by the surface area. Decontamination by μE, $\alpha = 0.5$ and $\gamma = 0.3$ has increased the original charge density of contaminated soil (0.0079 meq m^{-2}) by a factor of 1.6 and 1.8, for CME and PME, respectively.

Conclusions

Phase diagrams of the present (multi-components) systems exhibit some of the features of single-components systems, and also some noticeable differences, for example, formation of emulsions and separation of 1ϕ domains by Lα regions. Viscosity measurements, X-ray diffraction, QELS, IFT, and contact angles have shown the presence of bi-continuous phases at temperatures not far from ambient: 37.5 and 42.5 °C, for CME and PME, respectively. At the former temperature, the efficiency of the 1ϕ solutions in soil decontamination is higher than that of hot toluene. Shorter-chain oils, CME and PME, are more efficient than a longer chain oils, RME. Soil decontamination has increased its bioavailability.

Acknowledgements We thank FAPESP for financial support, and CNPq for a pre-doctoral research fellowship to M.B., and a research productivity fellowship to O.A.E.S., G.S. and M.J.S. thank the German Ministry for Education and Research for support. We thank M. Magalhões (IF-USP), S. Toffoli, A.C. Coelho (EP-USP), A.C. Bonomi (IPT), D. Siqueira-Petri, and P.A.R. Pires (IQ-USP) for their help with X-ray diffraction, BET, contact angle, and QELS measurements, respectively. This work has been carried out within the frame of bilateral Cooperation in Science and Technology between Brazil and Germany (Projects 91.0252/95-9, BRA F2A 6 J).

References

1. Lee JF, Mortland MM, Boyd SA, Chiou CT (1989) J Chem Soc Faraday Trans 1 85:2953
2. Hesketh N, Jones MN, Tipping E (1996) Anal Chim Acta 327:191
3. Wilson DJ, Clarke AN, Clarke JH (1988) Sep Sci Technol 23:991
4. Darian ST, Weinberg SP (1990) Patent WO90/06795
5. Loibner AP, Mayrhuber E, Gartner M, Braun R (1996) In: Stegmann R (ed) In-situ-Sanierung von Böden. Dechema, Frankfurt, p 411
6. Mihelcic JR, McNally DL, Lueking DR (1995) In: Sabatini DA, Knox RC, Harwell JH (eds) Surfactant-enhanced subsurface remediation, ACS Symposium Series, vol 594. American Chemical Society, Washington, p 112
7. Hamby DM (1996) Sci Total Environ 191:203
8. Kowalski S (2000) Ph D Thesis, Heinrich-Heine University, Düsseldorf
9. Bonkhoff K, Schwuger MJ, Subklew G (1997) In: Solans C, Kunieda H (eds) Industrial applications of microemulsions, surfactant science series, vol 66. Marcel Dekker, New York, p 355
10. Clemens W, Haegel F-H, Schwuger MJ, Soeder C, Stickdorn K, Webb L (1994) Patent WO94/04289
11. Mönig K, Haegel F-H, Schwuger MJ (1996) Tenside Surf Det 33:228
12. Mönig K, Clemens W, Haegel F-H, Schwuger MJ (1998) In: Shah DO (ed) Micelles, microemulsions, and monolayers: Science and Technology. Marcel Dekker, New York, p 215
13. Perrin DD, Armarego WLF (1988) Purification of laboratory chemicals. Pergamon, New York
14. Kessler MA, Wolfbeis OS (1989) Chem Phys Lipids 50:51
15. Haegel F-H, personal communication
16. Markley KS (1961) Fatty acids; their chemistry, properties, production and uses, 2nd edn, part 2. Interscience, New York
17. Ast HJ (1963) Anal Chem 35:1539
18. Tan BK, Hamilton RJ (1981) J Am Oil Chem Society 58:1
19. American Oil Chemists Society (1990) Official and recommended methods of sampling and analysis of commercial fats and oils. American Oil Chemists Society, Champaing, USA
20. Kahlweit M, Strey R, Firman P (1986) J Phys Chem 90:671
21. Kahlweit M, Strey R, Haase D, Firman P (1988) Langmuir 4:785
22. Koppel DE (1972) J Chem Phys 57:4841
23. Hiemenz PC, Rajagopalan R (1997) Principles of colloid and surface chemistry, 3rd edn. Marcel Dekker, New York, p 193
24. Kutschmann E-M, Findenegg GH, Nickel D, v Rybinski W (1995) Colloid Polym Sci 273:565
25. Aveyard R, Binks BP, Mead J (1987) J Chem Soc Faraday Trans 1 83:2347
26. Adamson A (1990) Physical chemistry of surfaces, 5th edn. Wiley and Sons, New York, p 389
27. Siqueira-Petri DF, Wenz G, Schunk P, Schimmel T (1999) Langmuir 15:4520
28. Brunauer S, Emmett PH, Teller E (1938) J Am Chem Soc 60:309
29. Rytwo G, Serban C, Nir S, Margulies L (1991) Clays Clay Min 39:551
30. Cardoso SRF, Angeleri FB, Santos HS, Aumond JJ, Santos PS (1992) Cerâmica 38(254):21
31. Claesson PM, Kjellander R, Stenius P, Christenson HK (1986) J Chem Soc Faraday Trans 1 82:2735
32. Golubovic L, Lubensky TC (1990) Phys Rev A 41:4343
33. Mönig K (1997) Ph D Thesis, Heinrich-Heine University, Düsseldorf
34. Kahlweit M, Strey R (1985) Angew Chem Int Ed Engl 24:654 and references cited therein
35. Schubert K-V, Kaler EW (1996) Ber Bunsenges Phys Chem 100:190 and references cited therein
36. Evans DF, Wennerström H (1994) The colloidal domain. VCH, New York, p 451 and references cited therein

37. Kunieda H, Yamagata M (1993) Langmuir 9:3345
38. Martino A, Schick M, Kaler EW (1990) J Chem Phys 93:8228
39. Stubenrauch C, Mehta SK, Paeplow B, Findenegg GH (1998) Progr Colloid Polym Sci 111:92
40. Ninham BW, Chen SJ, Fennell Evans D (1984) J Phys Chem 88:5855
41. Yoshino N, Sugiyama A, Okabayashi H, Taga K, Yoshida T, Kamo O (1992) Colloid Surf 67:67
42. Fennell Evans D, Mitchell DJ, Ninham BW (1986) J Phys Chem 90:2817
43. De Gennes PG, Taupin C (1982) J Phys Chem 86:2294
44. Tabony J (1986) Nature 319:400
45. Tabony J (1986) Nature 320:338
46. Kumar C, Balasubramamian D (1979) J Colloid Interface Sci 69:271
47. Chang NJ, Kaler EW (1986) Langmuir 2:184
48. Kahlweit M, Strey R, Haase D, Kunieda H, Schmeling T, Faulhaber B, Borkovec M, Eicke HF, Busse G, Eggers F, Funck Th, Richmann H, Magid L, Söderman O, Stilbs P, Winkler J, Dittrich A, Jahn W (1987) J Colloid Interface Sci 118:436
49. Talmon Y, Prager S (1978) J Chem Phys 69:2984
50. Olsson U, Shinoda K, Lindman B (1986) J Phys Chem 90:4083
51. Ruckenstein E (1978) Chem Phys Lett 57:517
52. Testard F, Zemb Th (1999) J Colloid Interface Sci 219:11
53. Langevin D (1988) Acc Chem Res 21:255
54. Reed RL, Healy RN (1984) Soc Petrol Eng J 24:342
55. Liu Z, Edwards DA, Luthy RG (1992) Wat Res 26:1337 and refs cited therein
56. Cione APP, Neumann MG, Gessner F (1998) J Colloid Interface Sci 198:106
57. The microscopic polarity scale of a solvent, e.g., $E_T(33)$ in kcal mol^{-1}, refers to the difference between the solvation energies of the ground and exited states of a solvatochromic probe, as calculated from $E_T(33) = 28591.5/\lambda_{max}$ (nm), where λ_{max} refers to the position of the intramolecular charge-transfer band of the probe employed [14]
58. Johnston CT (1996) In: Shawney B (ed) Organic pollutants in the environment, CMS workshop lectures, vol 8. The Clay Minerals Society, Boulder, p 1
59. Rao PSC, Lee LS, Wood AL (1991) Solubility, sorption, and transport of hydrophobic organic chemicals in complex mixtures, EPA/600/M-91/009, Ada, OK